

# Vectorized Adaptive Histograms for Sparse Oblique Forests

Ariel Lubonja

ariel@cs.jhu.edu

Johns Hopkins University

Baltimore, Maryland, USA

Jungsang Yoon

jyoon72@jh.edu

Johns Hopkins University

Baltimore, Maryland, USA

Haoyin Xu

hxu36@jhu.edu

Johns Hopkins University

Baltimore, Maryland, USA

Yue Wan

ywan23@jh.edu

Johns Hopkins University

Baltimore, Maryland, USA

Yilin Xu

yxu233@jh.edu

Johns Hopkins University

Baltimore, Maryland, USA

Richard Stotz

richardstotz@google.com

Google

Zurich, Switzerland

Mathieu Guillame-Bert

gbm@google.com

Google

Zurich, Switzerland

Joshua T. Vogelstein

jovo@jh.edu

Johns Hopkins University

Baltimore, Maryland, USA

Randal Burns

randal@cs.jhu.edu

Johns Hopkins University

Baltimore, Maryland, USA

## Abstract

Classification using sparse oblique random forests provides guarantees on uncertainty and confidence while controlling for specific error types. However, they use more data and more compute than other tree ensembles because they create deep trees and need to sort or histogram linear combinations of data at runtime. We provide a method for dynamically switching between histograms and sorting to find the best split. We further optimize histogram construction using vector intrinsics. Evaluating this on large datasets, our optimizations speedup training by 1.7-2.5× compared to existing oblique forests and 1.5-2× compared to standard random forests. We also provide a GPU and hybrid CPU-GPU implementation.

## ACM Reference Format:

Ariel Lubonja, Jungsang Yoon, Haoyin Xu, Yue Wan, Yilin Xu, Richard Stotz, Mathieu Guillame-Bert, Joshua T. Vogelstein, and Randal Burns. 2026. Vectorized Adaptive Histograms for Sparse Oblique Forests. In *Proceedings of .* ACM, New York, NY, USA, 8 pages. <https://doi.org/10.1145/nnnnnnn.nnnnnnn>

## 1 Introduction

Random Forests (RF) and other tree ensembles remain highly popular for biomedical and tabular data. They are orders of magnitude cheaper and faster to train and run than large-language models and achieve state-of-the-art performance for large tabular datasets [11, 17, 23]. RFs also offer unmatched interpretability and learn with a limited number of samples [10].

Sparse oblique (SO) splitting methods improve the accuracy of RF [24]. RF [3] selects a random subset of features at each node and evaluates which feature best separates the data. Contrary to RF,

sparse oblique forests sample many random projections, consisting of one (equivalent to RF), or a sparse subset of features [24]. The stochasticity and greater expressivity of the projections makes sparse oblique trees robust to noise and on average leads to more balanced trees [24].

However, sparse oblique splits present computational challenges. Unlike a regular, feature axis-aligned decision tree, where the feature set remains constant throughout training, oblique random projections must be performed at runtime: at each node, projection features are randomly sampled, their linear combination is calculated, and the resulting new “feature” is scanned for the best split. There are combinatorially many such splits in the number of features. This precludes strategies such as pre-sorting features for exact splits [12, 29], histogram subtraction [6, 14], or symmetric trees [21].

Our research goal was to accelerate sparse oblique forests for classification of biomedical data [8, 9] (see Background 2). These techniques train trees to purity—each leaf node represents a single class. This creates deeper trees than most random forest or gradient boosted tree applications, which stop tree construction at a specified depth or at a minimum node cardinality [6, 21]. Thus, sparse oblique forests process many small nodes with low cardinality, yet surprisingly, these deep nodes use only a small fraction of the total runtime when trained with exact splits (Figure 1).

Figure 1 reveals histograms for approximate splitting and sorting for exact splitting have different costs at different levels in the tree. Conventional wisdom is that histograms are faster, require less memory, and perform favorable sequential memory access [12, 21]. While this is true for nodes higher in the tree with many active samples—the  $O(n \log n)$  complexity of sorting dominates the  $O(k + n \log k)$  cost of filling a  $k$ -bin histogram—down the tree, when the number of active samples in each node becomes small and the number of nodes grows large, the fixed cost of allocating and initializing histograms dominates. This leads to the core idea of using histograms for high cardinality nodes and sorting for low cardinality nodes. The resulting dynamic histograms track the best performance of both splitting methods. Although adaptively switching between the two techniques changes the algorithm,

Permission to make digital or hard copies of all or part of this work for personal or classroom use is granted without fee provided that copies are not made or distributed for profit or commercial advantage and that copies bear this notice and the full citation on the first page. Copyrights for components of this work owned by others than the author(s) must be honored. Abstracting with credit is permitted. To copy otherwise, or republish, to post on servers or to redistribute to lists, requires prior specific permission and/or a fee. Request permissions from [permissions@acm.org](mailto:permissions@acm.org).

© 2026 Copyright held by the owner/author(s). Publication rights licensed to ACM.  
ACM ISBN 978-x-xxxx-xxxx-x/YYYY/MM  
<https://doi.org/10.1145/nnnnnnn.nnnnnnn>

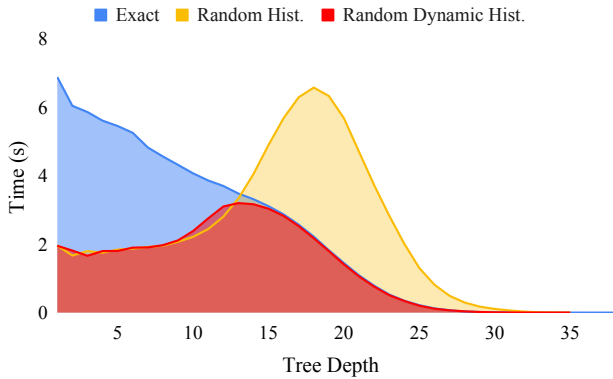


**Figure 1: Training runtime by tree depth on a dataset with 1M samples 4096 features. We compare exact splitting using sorting, approximate splitting using histograms, and our dynamic method that adaptively chooses between them.**

we reveal only minor variances in accuracy from either splitting technique.

We implemented MIGHT [8, 9] on the Yggdrasil Random Forest (YDF) [12] implementation of sparse oblique forests and optimized YDF for wide-tables and many samples. YDF is the fastest known RF training software and is performance competitive with gradient-boosted trees [12]. YDF’s C++ implementation allows us to manually vectorize code using intrinsic functions, and use CUDA for GPU acceleration. YDF’s implementation was not designed for a large number of features and had inefficiencies in sampling. We addressed this (Appendix A.1) and that improvement serves as a baseline for this work. Building on this implementation, we contribute:

- (1) *Runtime-adaptive histograms.* The recursive invocation of node-splitting in YDF is processed by sorting or a histogram depending upon node cardinality. A simple microbenchmark evaluates the crossover point on the local architecture and is run once before training the entire forest. This results in a  $1.2\times$ - $1.5\times$  speedup during training.
- (2) *Vectorization of histogram construction.* Discretizing projections into histograms updates the bucket count associated with each data sample. YDF routes each point based on a binary search of the (default 255) bucket boundaries.<sup>1</sup> We replaced the binary search with two SIMD vector compares using 7 total instructions, producing a  $2\times$  improvement in histogram construction and overall  $1.5\times$  speedup.
- (3) *Hybrid GPU/CPU:* We dynamically dispatch processing to a GPU on a node-by-node basis. GPUs are faster for the largest nodes but have a small-fixed cost for kernel invocation. They complement CPUs that better evaluate small, deep nodes. Benefits vary by dataset and are up to 40% improvement.

Overall, this results in a more than  $1.67$ - $2.5\times$  speedup on CPU alone and slightly more with GPU acceleration. Speedups improve as data gets wider (more features) and larger (more samples). We also

<sup>1</sup>Bin boundaries are sampled at random-width intervals to handle non-uniformity in the data.

find that our improved sparse oblique YDF implementation is faster than YDF’s axis-aligned RF, which is limited to exact splits. An open-source implementation is available at (anonymized).

## 2 Background

The MIGHT algorithm [8, 9] gives provable guarantees on uncertainty and confidence while controlling for specific error types. This is particularly valuable in biomedical applications, such as cancer screening, in which false positives are minimized in favor of false negatives. These methods use sparse oblique random forests [24] as a base non-parametric learning algorithm and add canonical cross validation and parametric calibration. The MIGHT algorithm results in coefficients of variation orders of magnitude less than transformers, support vector machines, or random forests at the same or better sensitivity [9].

To realize these guarantees, MIGHT defines a workload that is more data and compute intensive than gradient-boosted trees (GBT) or random forests (RF). MIGHT divides the bootstrap sample into three sets for training, calibration, and validation. MIGHT enhances the standard random-forest algorithm to:

- (1) evaluate sparse, random combinations of variables at each tree node to find splitting features.
- (2) train each tree to *purity* so that each leaf node in the tree contains training samples data from a single class.
- (3) estimate classification probabilities at each node by fitting posteriors on the calibration set.
- (4) score samples from the validation set using kernel prediction [22].

The original implementation of MIGHT was built on the scikit-learn toolkit [15, 19] and took over 8 hours to train on the Wise-1 dataset with 2523 features and 352 data points. Our goal is to train a classifier for an upcoming dataset with  $>440,000$  gene expression features, necessitating this work.

## 3 Related Work

Mainstream tree ensembles search dataset features for the one that best splits the classes. These splits, done exclusively in the range of the chosen feature, are termed axis-aligned. Random forest methods use exact splits by sorting [29] or by both sorting and histogramming [12, 19]. Most gradient-boosted tree methods rely on histograms [13, 14, 20, 21, 26], although some provide both [6, 19, 26]. To our knowledge, no existing method dynamically chooses the optimal method per node during training.

Oblique decision trees replace axis-aligned thresholds with linear combinations of sparse subsets of features, increasing expressivity and leading to shallower trees.

As datasets increase in complexity, tree ensembles focus on scaling tree ensembles to wide data with many features and large data with many samples. Ranger [29] implemented parallel, multi-threaded training and combined pre-sorted data for high-cardinality nodes with in-node sorting for small nodes. YDF [12] extends this method to data that exceeds memory capacity.

Presorting data [6, 12, 19, 26] ensures that samples of a feature after splits remain sorted. This is critical when dealing with large datasets. This cannot be applied to sparse oblique forests, as projections are sampled per-node.

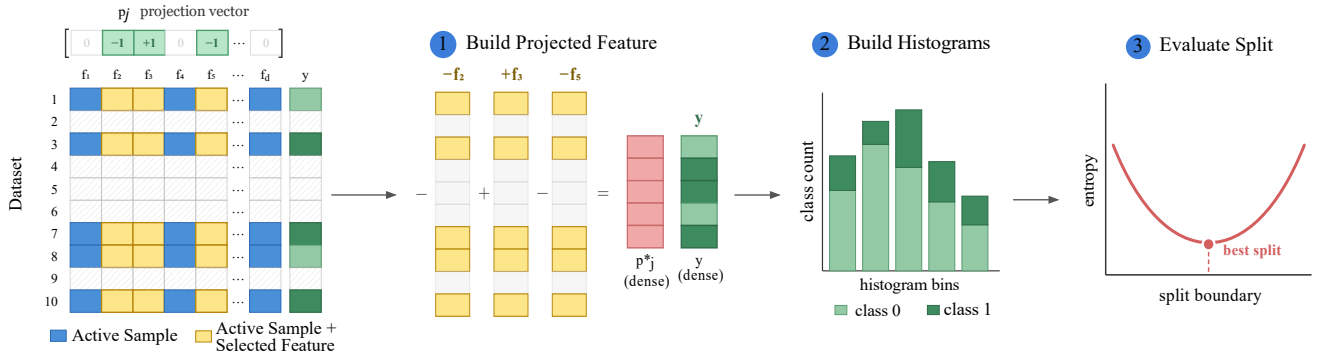


**Figure 2: Workflow at each tree node. Histogram splitting of a random linear combination of features requires sparse access in both rows and columns, computing a vector sum, building histograms and evaluating split boundaries.**

Inference performance optimization of RF and GBT includes: trees being compiled into C++ [7, 13] to improve memory layout and reduce branching and into tensor operations [18]. Cache-efficient memory layouts have been applied to nodes in multiple trees to reduce random I/O [4, 16].

GPU implementations of tree-ensembles employ histogram optimizations. Histogram subtraction in XGBoost [6], LightGBM [14], and RAPIDS [13] computes histograms for one side of a split and infers the other side. Symmetric trees in CatBoost [21] split all nodes at the same level using the same features and can compute histograms for all nodes in a single pass over a feature. ThunderGBM increases parallelism by assembling partial histograms in each thread-block and aggregating [26]. Since these optimizations require knowing the feature set beforehand, none can be applied to sparse oblique forests.

## 4 Method

We identified bottlenecks and optimization opportunities in sparse oblique YDF (SO-YDF) by implementing full timing instrumentation. We did this for histograms and exact splits and measured at all nodes in the tree. The computation at each node involves trying many linear combinations of features to identify the best splitting features. The first step is to build a projections matrix: a sparse list that samples with replacement  $3\sqrt{d}$  non-zero offsets from a matrix of  $d$  features by  $1.5\sqrt{d}$  rows and randomly assigns weights. Then for each row in the projection matrix, we evaluate the quality of the combination (Figure 2):

- (1) Build the feature by combining the active samples of the data column for the non-zero offsets and apply weights. This is a sparse vector-sum of, on average,  $1.5\sqrt{d}$   $n$ -row columns that returns a dense vector.
- (2) Build a histogram of the projected feature that assigns samples to bins and counts the class instances in each bin.
- (3) Evaluate a splitting criteria (entropy in YDF) at each split and return the boundary that best separates the data.

The sparsity of data access in the workload evolves down the tree and is present in both features (columns) and active samples (rows).

The latter is a key concept. At the root tree node, this is the bootstrapped training subset, representing 50-80% of the original samples. Each node splits these samples to maximize class purity. SO-YDF uses a columnar representation of data, i.e. individual features are stored sequentially. YDF does not reorganize the table or materialize data in each node.

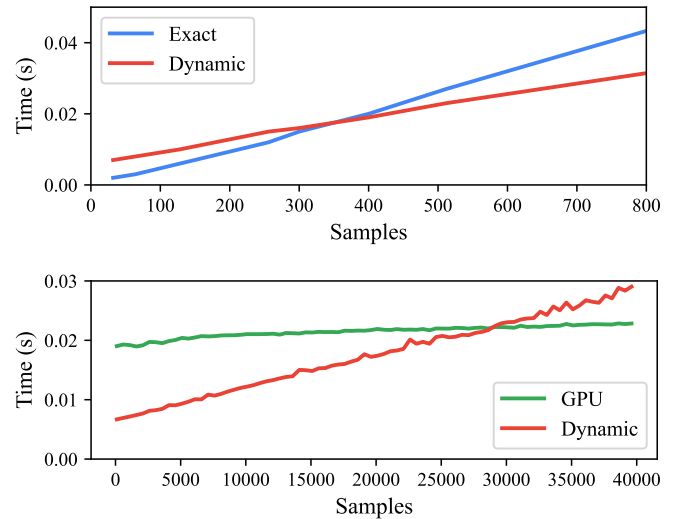


**Figure 3: Microbenchmarks to evaluate crossover points on a CPU machine (top) and GPU machine (bottom). Dynamic histograms outperform exact splits for  $n > 350$ . GPUs have high startup costs and improve performance for  $n > 29000$ .**

### 4.1 Dynamic Histogramming

Our study revealed performance concerns when training SO-YDF trees to purity. When the number of active samples is small, histogram construction dominates runtime. There are fixed costs to set up a histogram and these are incurred at each node. Referring back to Figure 1, histograms operate relatively much faster at the

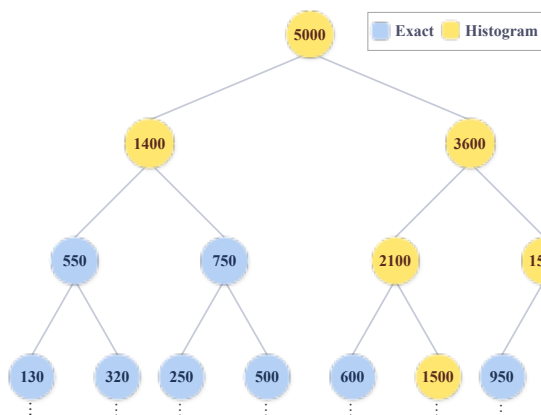


**Figure 4: Illustration of the selection of exact splitting and histogram splitting as a function of the number of active samples in a tree node with a breakeven point of 1300.**

top levels of the tree when the number of samples are large. These benefits endure through the first 12-13 levels of the tree on a 1M-row balanced dataset. Below this level, there are many active nodes, each of which requires a histogram. Here, sorting few samples can be much faster than building a histogram. Implementations of `std::sort()` have many optimizations to sort few elements, including unguarded insertions.

The breakeven point depends on the number of active samples and the hardware. Tree depth is just our proxy for visualizing the total runtime. Figure 3 show the relative cost of exact splits versus histograms on server CPU, showing a breakeven point of just over 1200 points. We also include the GPU results that show when it is beneficial to offload a computation to a GPU when available. The break-even point is determined by a microbenchmark that runs at the start of training. This takes less than 100ms to perform a binary search over reasonable parameters.

During tree-construction, we dynamically choose between a histogram and sorting on a node-by-node basis. Two nodes at the same tree depth may use different techniques (Figure 4). From a performance standpoint, this solves the problem with creating deep trees. We avoid the overhead of sorting at high cardinality nodes and of histograms for low cardinality nodes. There is only a small performance penalty for training to purity. Nodes beyond depth 20 use less 5% of the runtime (Figure 3).

Dynamic histograms produce different trees and potentially different learning outcomes. The resulting forests are most similar to those constructed by histograms. The high levels of the trees are the same. They differ only in the low cardinality nodes when exact splitting chooses a boundary that separates elements that are in the same bucket. The accuracy of all methods; histograms, exact, and dynamic, are statistically indistinguishable.

## 4.2 Vectorization of Histogram Filling

For high cardinality nodes, filling histograms is the most expensive step. This is the only computation that is linear in the input size. Figure 5 shows the relative cost of the different components of

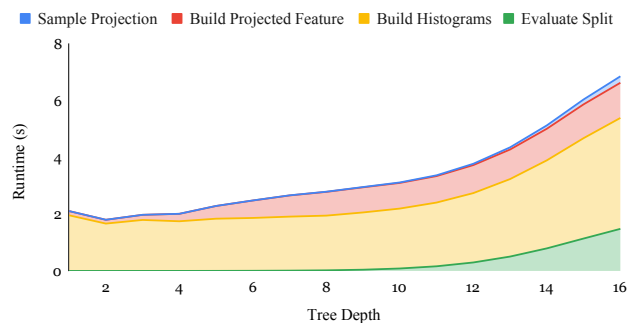


**Figure 5: Comparative runtime of the different components of computation for histogram splitting. The dataset has 1M samples and 4096 features.**

the computation at tree nodes that build histograms. Histogram construction dominates computation. Although sparse memory access takes more time deeper in the tree and may be another opportunity for optimization.

YDF’s implementation of histograms uses C++ `std::upper()` to conduct binary search among the bin boundaries to identify a bin in to which to update a count for a class. In addition to taking steps logarithmic in the number of bins, the branches in binary search are taken with equal probability, have low predictability, and result in pipeline stalls. An alternative is to scan the bins, which has higher predictability, but performs more work. Scanning is better for small histograms up to 16 or 32 bins.

Tree ensembles choose a modest number of bins that balance computation and space versus overfitting the data. Inaccuracies from fewer bins can be resolved deeper in the tree or in other trees. Default values are as low as 20 (H2O) or 32 (Spark MLlib), but are most often 255 or 256 (YDF, CatBoost, XGBoost).

We observe that a data point can be routed into one of 256 bins using two 16-word wide SIMD vector compares. The concept is to break the boundaries into 16 groups of 16. We do a coarse-grained compare to select the group and a fine-grained compare to locate the bin. The data structure resembles a two-level deterministic skip list. Once per histogram, we construct a coarse-grained vector that describes the boundary of every 16<sup>th</sup> bin. For each point, we broadcast the search value to a 16-wide vector and perform a parallel compare of all elements.

We also provide a 64 bin, 8-bit wide AVX-2 implementation. Figure 6) compares the AVX-implementation with binary search over 64 bins. The binary search uses 7 instructions with one branch per node for a minimum of 42 serial instructions and likely several missed branch predictions. AVX-2 broadcasts the search value to a vector. Does a parallel compare and resolves the coarse grained bin using a mask and count intrinsic. It repeats this at a finer grain for a total of 16 instructions.

## 4.3 Hybrid GPU-CPU Implementation

We extend the dynamic dispatch of tree nodes to sending the largest tree nodes to a GPU. Our implementation is limited to node-at-a-time invocation of GPU kernels. This matches YDF’s recursive

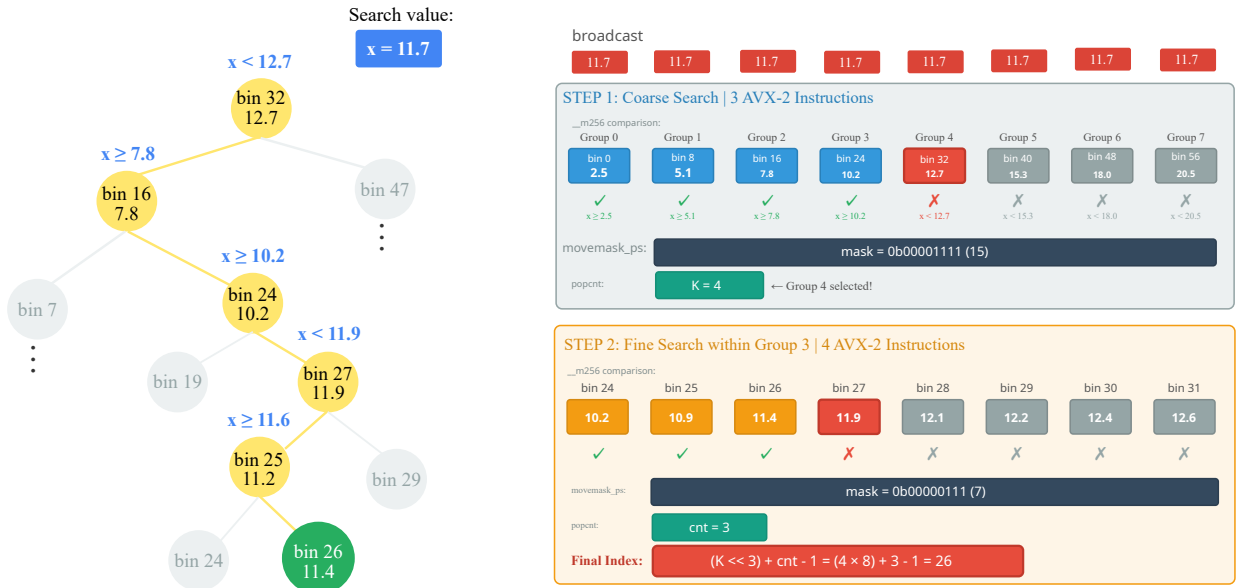


Figure 6: Mapping sample points to histograms using binary search (default, left) and our vectorized implementation (right).

call structure. Also, given that each node has to materialize many different projections with different numbers of active samples, it is difficult to have a single kernel run multiple nodes. Our efforts to run multiple nodes in one kernel introduce skew, have poor data-access sharing, and run into shared-memory limits.

Our GPU computation for a node returns the best split among all projections using histograms, computing the exact same result as the CPU. Prior to training, we preload the entire dataset onto GPU device memory. This is a one-time cost. Then for each node, SO-YDF on the CPU chooses to invoke a GPU kernel or compute the histograms or exact splits locally. For the GPU, the tradeoff point depends on the number of projections computed as well as the relative speed of the hardware. Each kernel invocation has a fixed cost that gets amortized by more computation.

Our GPU implementation takes as input a pointer to list of indices that are the non-zero values in the projection matrix<sup>2</sup> and returns the projection that provides the best split and the split itself. First, we copy the list of projection indices to device memory. Then we invoke a kernel to: *apply projections*: sum the columns and write the new sparse oblique features; and *construct histograms*: one for each projection. This kernel uses shared-memory to for histogram buckets counts that read and written multiple times. A second kernel *evaluates the best split* in each histogram, takes the best split among all projections and returns the feature (projection) and splitting value. For the first kernel, we assign CUDA threads to a grid of dimension (# of projections, # of active samples). The second kernel grid has dimension (# of projections, # of histogram bins). We explored fusing these into a single kernel to reduce invocation overhead, but found no performance benefit and lower resource utilization as there are many idle threads in the second phase.

<sup>2</sup>While it is possible to sample the projections on the GPU, this is not an expensive computational step and provided no speedup.

Name	Type	Samples	Features	Classes	Model
HIGGS [27]	Real	1100000	28	2	4.9GB
SUSY [28]	Real	5000000	18	2	11.8GB
Epsilon [5]	Real	400000	2000	2	3.6GB
Trunk [25]	Synthetic	-	-	2	-

Table 1: Experimental datasets.

## 5 Results

We conduct experiments to quantify the performance improvement of dynamic histograms and vectorization at scale on a multicore CPU machine. We also examine GPU acceleration. Then, scalability results show that SO-YDF training is compute bound on the CPU. Finally, we report accuracy on benchmark datasets.

**Datasets:** For performance experiments, we choose the largest and widest datasets for two-class RF-classification from the UCI Machine Learning Library and from Kaggle (Table 1. Large RF datasets tend to be real-valued. The benefit of both dynamic histograms and vectorization scales with the number of samples (rows). Thus, high count, low-dimensional datasets are a reasonable proxy for large-wide data. The GPU acceleration also scales with the number features and benefits from data that are both wide and large. We include synthetic Trunk data [25]: a generator that scales features and samples according to a  $p$ -dimensional multivariate Gaussian, while generating 2 balanced classes [24].

For accuracy experiments, we include data from the OpenML CC18 benchmarks [2] that include categorical and text data. None of these are large enough for meaningful performance experiments.

Dataset	Exact	Dynamic Hist. (256-bins)	Vectorized Dyn. Hist. (256-bins, AVX-512)
Higgs	663.66	449.48	341.28
SUSY	245.49	161.45	116.34
Epsilon	107.52	85.14	69.00
Trunk-1M	408.56	301.99	242.67

Table 2: End-to-end CPU training time (s) of a 240-tree forest.

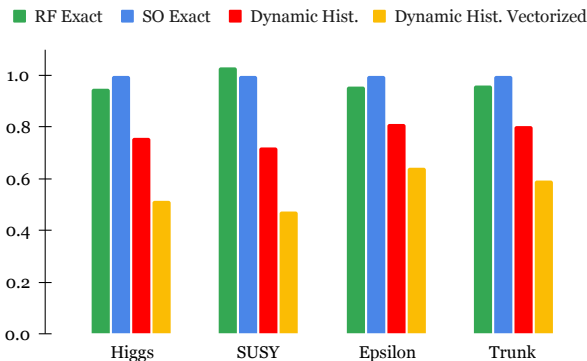


Figure 7: End-to-end training time normalized to the performance of SO-YDF with exact splits.

## 5.1 Dynamic Vectorized Histograms

Experiments were run on a AWS m7i.metal-24xl instance with 48 physical cores 384 GiB of memory running Ubuntu 24.04. YDF is compiled with ICX version 2025.2.1 with AVX-512 support (`-AVX-512`). Experiments run a thread pool of 48 workers threads and train 1024 trees. Results are an average of 20 trials.

Our core result shows that dynamic histograms with vectorization consistently reduce end-to-end runtime relative to the SO-YDF exact baseline and that the advantage grows with the number of samples (Table 2). We present the same data normalized to the performance of SO-YDF to show the percentage improvement (Figure 7). We isolate the performance benefit of dynamic histograms alone from dynamic with vectorization. When training full-depth trees on all 48 cores, dynamic histograms deliver a 20-30% reduction in runtime versus YDF-SO exact and vectorization adds another 20-30%. The overall improvement is more than a factor of 2 on the larger datasets (Higgs and SUSY). We also include results comparing with axis-aligned random forests to show that sparse oblique training can be completed as fast or faster. We do not show histograms methods for RF or SO because they are 2-4 times slower than exact when training to purity.

## 5.2 Hybrid CPU-GPU

Experiments were run on a AWS instance with a 16-core Intel Xeon Platinum 8559C processor and a NVIDIA RTX PRO 6000 Blackwell Server Edition GPU. The machine ran Ubuntu 24.04 and YDF was compiled using GCC 13.3 with flags `-CUDA` and `-AVX-512`. Experiments use a thread pool of 16 worker threads and map

Dataset	CPU (s)	GPU (s)	Improvement (%)
HIGGS	453.48	408.14	11.10%
SUSY	150.72	140.90	6.95%
Epsilon	103.70	102.93	0.75%
Trunk-100k	31.09	30.43	2.02%
Trunk-1M	348.35	319.47	9.04%
Trunk-10M	1061.73	1754.71	39.49%

Table 3: End-to-end training time of a 128-tree forest on a GPU-enabled machine.

each thread to a CUDA stream to run GPU kernels concurrently. Experiments train 128 trees. Results are an average of 5 trials.

On our evaluation datasets, GPU acceleration provides modest gains, up to 11% for HIGGS (Table 3). Compute work is  $O(n\sqrt{d})$  for  $n$  rows and  $d$  columns. The GPU only accelerates the largest nodes at the top of the trees. GPU provides more benefit on larger and wider datasets. We scaled our Trunk synthetic data to 10M rows and GPU reduced runtime by almost 40%. GPU offload will become more valuable as we target larger and wider datasets.

## 5.3 Scalability

These experiments use the same configuration as Hybrid GPU/CPU (Section 5.2).

Examining speedup reveals that SO-YDF training is compute bound on the CPU. Figure 8 shows near perfect scaling for vectorized dynamic histograms. This is somewhat surprising given that deep trees perform sparse memory access to feature columns. The results at 32 threads on 16 cores show no additional speedup and actually lose a little performance, likely from threads interfering in processor caches. When using the GPU, we are still CPU bound for this datasets. There is no scaling when the number of threads exceed the number of CPU cores. On this benchmark, GPU occupancy never exceeded 70%. Larger datasets shift the bottleneck to the GPU.

## 5.4 Accuracy Comparison

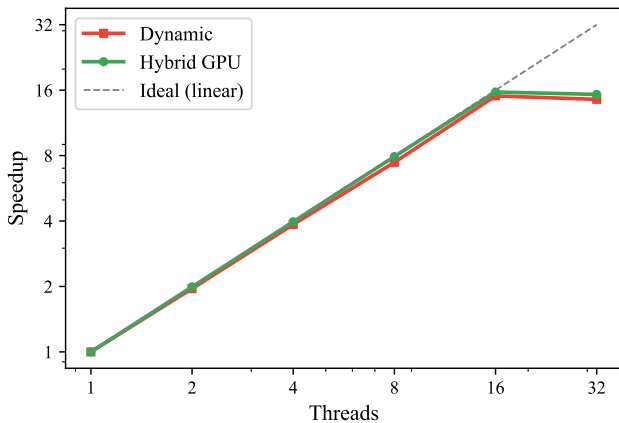
We quantify the effect of dynamic histograms on the accuracy of classification tasks across our performance datasets and a selection of smaller OpenML datasets (Table 4). All methods were given the same number of trees. The accuracy of dynamic histograms tracks histograms in SO-YDF and in most cases performance is indistinguishable. The differences between dynamic and histograms is on the same order as the variance between exact and histograms.

## 6 Conclusions and Discussion

We present vectorized adaptive histograms to accelerate sparse oblique random forest training. By dynamically selecting between exact and histogram-based splitting by node cardinality and replacing binary search with SIMD vector comparisons for bin assignment, we achieve end-to-end training speedups of 1.7–2.5 $\times$  on large datasets while maintaining equivalent classification accuracy. Our hybrid CPU-GPU implementation provides additional gains of up to 40% on wide, large datasets. These optimizations make sparse

**Table 4: Accuracy of different training methods in SO-YDF. All methods were given 240 trees.**

	OpenML CC18 Datasets [2]							
	Higgs	SUSY	Epsilon	Bank	Phishing	Credit	Internet	Trunk 1m [25]
	11m, 28	5m, 18	400k, 2k	Marketing	Websites	Approval	Advert.	
				45211, 17	11055, 31	690, 16	3279, 1559	
Exact	75.7%	80.1%	74.6%	90.6%	97.4%	86.5%	97.7%	96.4%
Histogram (256-bin)	75.7%	80.1%	74.5%	90.6%	97.4%	86.3%	97.7%	96.4%
Dynamic Hist. (256-bin)	75.7%	80.1%	74.5%	90.6%	97.2%	86.3%	97.6%	96.4%
Dynamic Vectorized (AVX-512)	75.7%	80.1%	74.5%	90.6%	97.2%	86.3%	97.6%	96.4%

**Figure 8: Scalability for 1 to 32 threads running on 16 physical CPU cores and with GPU acceleration when training a forest on 100K samples and 4096 features.**

oblique forests practical for datasets with multi-million features, addressing a key computational barrier for algorithms like MIGHT. Future work will explore batching multiple tree nodes into single GPU kernels to extend acceleration to multiple smaller nodes.

## References

- [1] Jon Bentley and Bob Floyd. Programming pearls: a sample of brilliance. *Commun. ACM*, 30(9):754–757, September 1987.
- [2] Bernd Bischl, Giuseppe Casalicchio, Matthias Feurer, Pieter Gijsbers, Frank Hutter, Michel Lang, Rafael G Mantovani, Jan N van Rijn, and Joaquin Vanschoren. Openml benchmarking suites. *arXiv preprint arXiv:1708.03731*, 2017.
- [3] Leo Breiman. Random forests. *Machine learning*, 45(1):5–32, 2001.
- [4] James Browne, Tyler M. Tomita, Disa Mhembere, Joshua T. Vogelstein, and Randal C. Burns. Forest packing: Fast parallel decision forests. *IEEE Transactions on Computers*, 71(1):73–86, Jan 2022.
- [5] Chih-Chung Chang and Chih-Jen Lin. Libsvm: A library for support vector machines. *ACM transactions on intelligent systems and technology (TIST)*, 2(3):1–27, 2011.
- [6] Tianqi Chen and Carlos Guestrin. Xgboost: A scalable tree boosting system. In *Proceedings of the 22nd ACM SIGKDD International Conference on Knowledge Discovery and Data Mining*, KDD ’16, page 785–794, New York, NY, USA, 2016. Association for Computing Machinery.
- [7] Hyunsu Cho and Mu Li. Treelite: Toolbox for decision tree deployment, 2018.
- [8] Samuel D. Curtis, Tingshan Liu, Yuxin Bai, Yuxuan Wang, Sambit Panda, Adam Li, Haoyin Xu, Eliza O’Reilly, Lisa Dobbyn, Maria Popoli, Janine Ptak, Natalie Silliman, Chris Thoburn, Jeanne Tie, Peter Gibbs, Lan T. Ho-Pham, Bich N. H. Tran, Thach S. Tran, Tuan V. Nguyen, Maximilian F. Konig, Michelle Petri, Antony Rosen, Christopher A. Mecoli, Ami A. Shah, Frits Mulder, Nick van Es, PLATO-VTE Study Group, Chetan Bettgowda, Kenneth W. Kinzler, Nickolas Papadopoulos, Joshua T. Vogelstein, Bert Vogelstein, Christopher Douville, Frederikus A. Klok, Jan Beyer-Westendorf, Luis Jara-Palomares, Walter Ageno, Mike J.L. Peters, Aurélien Delluc, Myron Best, Noori Guman, Hans-Martin Otten, Frits Mulder, and Nick van Es. Fragmentation signatures in cancer patients resemble those of patients with vascular or autoimmune diseases. *Proceedings of the National Academy of Sciences*, 122(34):e2426890122, 2025.
- [9] Samuel D. Curtis, Sambit Panda, Adam Li, Haoyin Xu, Yuxin Bai, Itsuki Ogihara, Eliza O’Reilly, Yuxuan Wang, Lisa Dobbyn, Maria Popoli, Janine Ptak, Nadine Nehme, Natalie Silliman, Jeanne Tie, Peter Gibbs, Lan T. Ho-Pham, Bich N. H. Tran, Thach S. Tran, Tuan V. Nguyen, Ehsan Irajizad, Michael Goggins, Christopher L. Wolfgang, Tian-Li Wang, Ie-Ming Shih, Amanda Fader, Anne Marie Lennon, Ralph H. Hruban, Chetan Bettgowda, Lucy Gilbert, Kenneth W. Kinzler, Nickolas Papadopoulos, Bert Vogelstein, Joshua T. Vogelstein, and Christopher Douville. Minimizing and quantifying uncertainty in ai-informed decisions: Applications in medicine. *Proceedings of the National Academy of Sciences*, 122(34):e2424203122, 2025.
- [10] Manuel Fernández-Delgado, Eva Cernadas, Senén Barro, and Dinani Amorim. Do we need hundreds of classifiers to solve real world classification problems? *Journal of Machine Learning Research*, 15(1):3133–3181, January 2014.
- [11] Léo Grinsztajn, Edouard Oyallon, and Gaël Varoquaux. Why do tree-based models still outperform deep learning on typical tabular data? *Advances in neural information processing systems*, 35:507–520, 2022.
- [12] Mathieu Guillaume-Bert, Sebastian Bruch, Richard Stotz, and Jan Pfeifer. Yggdrasil decision forests: A fast and extensible decision forests library. In *Proceedings of the 29th ACM SIGKDD Conference on Knowledge Discovery and Data Mining, KDD 2023, Long Beach, CA, USA, August 6–10, 2023*, pages 4068–4077, 2023.
- [13] Mayuri Gupta, Ashish Mishra, Ashutosh Mishra, and Jayesh Gangrade. Accelerated gpu-based clustering, classification and regression using rapids: A comparative study. In *International Conference on Computation of Artificial Intelligence & Machine Learning*, pages 239–253. Springer, 2024.
- [14] Guolin Ke, Qi Meng, Thomas Finley, Taifeng Wang, Wei Chen, Weidong Ma, Qiwei Ye, and Tie-Yan Liu. Lightgbm: A highly efficient gradient boosting decision tree. *Advances in neural information processing systems*, 30, 2017.
- [15] Adam Li, Sambit Panda, Haoyin Xu, and Itsuki Ogihara. treepile: Modern decision-trees compatible with scikit-learn in python. <https://github.com/neurodata/treepile>, 2023. License: PolyForm-Noncommercial-1.0.0.
- [16] Meghana Madhyastha, Kunal Lillaney, James Browne, Joshua T. Vogelstein, and Randal Burns. BLOCKSET (block-aligned serialized trees): Reducing inference latency for tree ensemble deployment. In *Proceedings of the 27th ACM SIGKDD Conference on Knowledge Discovery and Data Mining*, pages 1170–1179. ACM, 2021.
- [17] Duncan McElfresh, Sujay Khandagale, Jonathan Valverde, Vishak Prasad C, Ganesh Ramakrishnan, Micah Goldblum, and Colin White. When do neural nets outperform boosted trees on tabular data? *Advances in Neural Information Processing Systems*, 36:76336–76369, 2023.
- [18] Supun Nakandala, Karla Saur, Gyeong-In Yu, Konstantinos Karanasos, Carlo Curino, Markus Weimer, and Matteo Interlandi. A tensor compiler for unified machine learning prediction serving. In *14th USENIX Symposium on Operating Systems Design and Implementation (OSDI 20)*, pages 899–917, 2020.
- [19] Fabian Pedregosa, Gaël Varoquaux, Alexandre Gramfort, Vincent Michel, Bertrand Thirion, Olivier Grisel, Mathieu Blondel, Peter Prettenhofer, Ron Weiss, Vincent Dubourg, et al. Scikit-learn: Machine learning in python. *the Journal of machine Learning research*, 12:2825–2830, 2011.
- [20] Natalia Ponomareva, Soroush Radpour, Gilbert Hendry, Salem Haykal, Thomas Colthurst, Petr Mitrichev, and Alexander Grushetsky. Tf boosted trees: A scalable tensorflow based framework for gradient boosting. In *Joint european conference on machine learning and knowledge discovery in databases*, pages 423–427. Springer, 2017.

- [21] Liudmila Prokhorenkova, Gleb Gusev, Aleksandr Vorobev, Anna Veronika Dorogush, and Andrey Gulin. Catboost: unbiased boosting with categorical features. *Advances in neural information processing systems*, 31, 2018.
- [22] Erwan Scornet. Random forests and kernel methods. *IEEE Transactions on Information Theory*, 62(3):1485–1500, 2016.
- [23] Ravid Shwartz-Ziv and Amitai Armon. Tabular data: Deep learning is not all you need. *Information Fusion*, 81:84–90, 2022.
- [24] Tyler M Tomita, James Browne, Cencheng Shen, Jaewon Chung, Jesse L Patsolic, Benjamin Falk, Carey E Priebe, Jason Yim, Randal Burns, Mauro Maggioni, et al. Sparse projection oblique randomer forests. *Journal of machine learning research*, 21(104):1–39, 2020.
- [25] G. V. Trunk and J. O. Coleman. Repeated hypothesis testing on a growing data set. *IEEE Transactions on Pattern Analysis and Machine Intelligence*, PAMI-4(3):343–345, 1982.
- [26] Zeyi Wen, Jiashuai Shi, Bingsheng He, Qinbin Li, and Jian Chen. ThunderGBM: Fast GBDTs and random forests on GPUs. *Journal of Machine Learning Research*, 21, 2020.
- [27] Daniel Whiteson. HIGGS. UCI Machine Learning Repository, 2014. DOI: <https://doi.org/10.24432/C5V312>.
- [28] Daniel Whiteson. SUSY. UCI Machine Learning Repository, 2014. DOI: <https://doi.org/10.24432/C54606>.
- [29] Marvin N Wright and Andreas Ziegler. ranger: A fast implementation of random forests for high dimensional data in c++ and r. *Journal of statistical software*, 77:1–17, 2017.

## A Appendix

### A.1 Floyd’s Projection Sampling

Originally, random sampling to build the projection matrix was a computational bottleneck for SO-YDF. This component comprised 80% of the runtime, with the math-heavy parts of the code taking <20%. The previous design assumed small  $d$  and was inefficient for wide data.

Existing code calls  $\text{Unif}(0,1)$  over the projection matrix to create a mask, then populates this mask with weights. However, this requires  $\Theta(np)$  calls to  $\text{Unif}(\cdot)$ , or  $p$  calls per each projection, across  $n$  projections. We show this can be substituted with a single call to  $\text{Binomial}(np, n\frac{k}{p})$ , cutting runtime by 33% for our settings, proportional to  $\Theta(np)$ .

Using a variant of an algorithm from Floyd [1], we form the projection matrix as follows:

```
projection_density = k/p;
for projection in projections: // O(n)
    for feature in features: // O(p)
        if (Unif01(.) < projection_density) {...}
```

Let  $z^n$  denote the actual number of successes from running this algorithm, i.e. the number of times the inner loop’s if condition evaluates to True. We need to show  $z^n \sim \text{Binomial}(np, n\frac{k}{p})$ :

- PROOF. (1) The probability of one true evaluation (success) of  $\text{if}(\text{Unif01}(\cdot) < \text{projection\_density}) \sim \text{Bernoulli}(\frac{k}{p})$  since  $\text{projection\_density} = \frac{k}{p}$ , and a success only occurs when a  $\text{Unif}(0,1)$  sample is  $< \frac{k}{p}$ .
- (2) Let  $z^i$  denote the number of successes for each projection, where  $i \in [0, n-1]$ .  $z_i \sim \text{Binomial}(p, \frac{k}{p})$  since by definition, a  $\text{Binomial}(1, \frac{k}{p}) = \text{Bernoulli}(\frac{k}{p})$ , and by the additive property of the Binomial,  $\sum_p \text{Binomial}(1, \frac{k}{p}) = \text{Binomial}(p, k)$ .
- (3) The same property extends to  $z^n = \sum_n z_i = \text{Binomial}(np, nk)$ .  $\square$